

# Ricci flow-guided autoencoders in learning time-dependent dynamics

Andrew Gracyk\*

January 2024

---

## Abstract

We present a manifold-based autoencoder method for learning nonlinear dynamics in time, notably partial differential equations (PDEs), in which the manifold latent space evolves according to Ricci flow. This can be accomplished by simulating Ricci flow in a physics-informed setting, and manifold quantities can be matched so that Ricci flow is empirically achieved. With our methodology, the manifold is learned as part of the training procedure, so ideal geometries may be discerned, while the evolution simultaneously induces a more accommodating latent representation over static methods. We present our method on a range of numerical experiments consisting of PDEs that encompass desirable characteristics such as periodicity and randomness, remarking error on in-distribution and extrapolation scenarios. Our code is available at <https://github.com/agracyk2/Ricci-flow-guided-autoencoders-in-learning-time-dependent-dynamics>.

---

## 1 Introduction

Data-driven techniques, fueled by machine learning, have become a useful tool in exploring partial differential equations (PDEs), such as in instances of finding solutions. A variety of frameworks have been developed with the purpose of finding approximations to time-dependent PDE solutions including encoder-decoder methods. Encoder-decoder methods are distinguished by a series of neural networks in which there exists an intermediate encoded space stage, which can be variously characterized, that is decoded to produce a PDE solution output. Geometric dynamic variational autoencoders (GD-VAEs) have shown great promise in learning discretized time-dependent dynamics [Lopez and Atzberger, 2022], which are highlighted by an underlying latent space with either geometric features or dynamics in the latent space itself. We focus on an encoder-decoder method, emphasizing a low-dimensional manifold latent space which is imposed with dynamical evolution, that also holds the advantages that GD-VAEs achieve, including competitive error, generalization, extrapolation ability, and robustness.

Examples of existing manifold-based encoder methods involve scenarios of data mapped to Euclidean space without structure, in which a projection onto a manifold is subsequently taken for decoding. This in itself requires an optimization problem to be solved per every iterate of the training procedure. Additionally, fixed geometries are possibly less than ideal for their compatibility with the PDE data, which potentially require trial and error to determine optimal latent structure, if found at all. Furthermore, evolution in the latent space has shown competitive performance over static methods [Lopez and Atzberger, 2022]. We propose a method in which no optimization problem per iterate is necessary, which incorporates manifold geometries with such evolution.

---

\*Correspondence to agracyk2@illinois.edu, andrewgracyk@gmail.com.

A geometric flow, the foundation of our method, is a tool to perform dynamics among the manifold, in which we choose Ricci flow. We first represent the initial PDE data in a domain to parameterize the manifold, which is then encoded directly to a point on the manifold. The points that compose this manifold evolve according to such a flow, in which we use a physics-informed neural network to simulate the evolution, matching quantities among the manifold to those that solve the physics-informed flow. Using neural networks to learn the manifold directly, we can learn implicit geometric features that accommodate the PDE data to an unmatched degree over geometries that are predetermined.

Ricci flow is an example of an intrinsic geometric flow, meaning the relevant quantities computed in the PDE flow are inherent to the manifold itself, and so the manner in which it is embedded in space is not involved in the PDE computation and is otherwise irrelevant. An extrinsic geometric flow is a flow equation in which the embedding impacts the informational quantities used in the PDE, and so the embedding does indeed matter and is factored into how the manifold evolves subject to the flow. The metric, a quantity inherent to the manifold, can be computed as an inner product of the tangent vectors [Millman and Parker, 1977]. The location of these tangent vectors can be arbitrarily changed in space in which the inner product is unchanged, assuming the relative positioning and scaling of these vectors is unaffected, making a PDE consisting of metric quantities an intrinsic flow.

Our method, captured by an intrinsic flow, is highlighted by this fact. This allows the manifold to displace through space, aside from the movements due to the flow, during its period of evolution. The embedding is irrelevant, and can change through the training procedure to maximize effectiveness in solving the objective function.

The intermediary stage of the parameterization domain acts similarly to the unstructured data in Euclidean space in the GD-VAE setting. These outputs are given heightened flexibility and permitted to lie in unrestricted subdomains before subsequently being mapped to the manifold. In this sense, our method applies no greater restrictions upon the latent space by using this middle step of unstructured data of the manifold’s parameterization, the only of which being this domain is one dimension lower than that of the embedding in which the unstructured data in the GD-VAE case is contained.

While the implicitly-learned latent space captured by an intrinsic flow allows high precision in the task of replicating data from the same underlying distribution as seen as part of the training procedure, a challenge resides in achieving precision in areas such as generalization of the data and extrapolation of data with fundamental qualities of those seen in training, but sufficiently different to be categorized as data that is extended outside of the training procedure. The manifold latent space offers promise in extending the autoencoder baseline to one that yields greater ability to infer dynamics from never-before-seen data, as well as incorporate features of the data into such a structure [Lopez and Atzberger, 2022].

## 2 Problem formulation

**Problem setting.** The task of interest is to learn the solution of a parameterized partial differential equation of the form

$$\partial_t \phi + \mathcal{D}_\alpha[\phi] = 0, \tag{1}$$

subject to initial data  $\phi(\cdot, 0) = \phi_0$ , where  $\phi : \mathcal{X} \times [0, T] \rightarrow \mathbb{R}$  is the solution, and  $\mathcal{D}_\alpha$  is a differential operator with parameter  $\alpha$ .  $\alpha$  may depend on evaluations over the input space  $\mathcal{X}$  as well as time  $t \in [0, T]$ . In particular, we seek a mapping

$$(\phi_0, t) \in C(\mathcal{X}; \mathbb{R}) \times [0, T] \rightarrow \phi_t \in C(\mathcal{X}; \mathbb{R}). \tag{2}$$

We devise an autoencoder framework, characterized by a latent space that consists of collections of points that lie directly along a continuum of manifolds  $\mathcal{M}_{\hat{\tau}}$  embedded in Euclidean space  $\mathbb{R}^d$ ,  $\hat{\tau} \in [0, \tau]$  for some  $\tau$ , to learn  $\phi_t$ .

**Ricci flow.** Ricci flow is a natural framework for accomplishing goals of incorporating input data features into manifold structure and generalization capability while allowing high precision in the task of producing the output. Ricci flow unites the separate features of an evolving latent space and a manifold latent space into a single scheme. Ricci flow is a partial differential equation that describes changes in the Riemannian metric. Let  $g_{ij} : \mathcal{U}^1 \times \mathcal{U}^2 \times \dots \times \mathcal{U}^m \times [0, \tau] \rightarrow \mathbb{R}$  be the components of the Riemannian metric matrix  $g$  over the manifold parameterization domain  $\mathcal{U}^1 \times \mathcal{U}^2 \times \dots \times \mathcal{U}^m = \mathcal{U}$  and a time domain  $[0, \tau]$ . Ricci flow is the metric evolution equation

$$\partial_t g(u, t) = -2\text{Ric}(g(u, t)), \quad (3)$$

for  $u \in \mathcal{U}, t \in [0, \tau]$ , such that the metric solved by 3 reflects that of the manifold  $\mathcal{M}_{\hat{\tau}}$  over its respective time interval. The solution to this PDE can be regarded as an  $m \times m$  matrix,  $g(u, t)$ , with components  $g_{ij}$ . The right-hand term  $\text{Ric}(g(u, t))$  is the Ricci tensor. Ricci flow is similar to a geometric diffusion equation in which curvature is uniformized, and geometries contract or expand.

**Metric coefficients.** The coefficients of the Riemannian metric,  $g_{ij}$ , can be computed using the tangent vectors to the manifold at a location corresponding to a point in the manifold parameterization domain and time domain  $\mathcal{U} \times [0, \tau]$ . The coefficients of the metric can be computed at general times as [Millman and Parker, 1977]

$$g_{ij}(u, t) = \langle \partial_i \mathcal{E}(u, t), \partial_j \mathcal{E}(u, t) \rangle, \quad (4)$$

where  $\partial_\ell$  is the component-wise partial derivative with respect to the  $\ell$ -index in  $u = (u^1, u^2, \dots, u^m)$  belonging to the parameterization domain  $\mathcal{U}$ , and  $\mathcal{E} : \mathcal{U} \times [0, \tau] \rightarrow \mathbb{R}^d$  is the function mapping to the manifold continuum. The Ricci flow PDE is primarily governed based on initial coefficients  $g_{ij,0}$ , but in our methodology, it of interest to compute the metric coefficients among arbitrary times  $\tilde{\tau}_i \in U([0, \tau])$  in a uniform collocation procedure. The behavior of the manifold is governed by the change of the metric coefficients under Ricci flow such that equation 4 holds.

**Ricci tensor.** Given explicit knowledge of the Riemannian metric coefficients, one may compute the Ricci tensor using Christoffel symbols and the Riemannian curvature tensor. The Christoffel symbols are a collection  $\{\Gamma_{ij}^l\}_{i,j,l}, 1 \leq i, j, l \leq d-1$  evaluated at particular  $(u_i, t_i)$ , given by [Millman and Parker, 1977]

$$\Gamma_{ij}^l = \frac{1}{2} \sum_{k=1}^{d-1} g^{kl} (\partial_j g_{ik} - \partial_k g_{ij} + \partial_i g_{kj}). \quad (5)$$

$g^{kl}$  denote the elements of the inverse matrix of  $g$  at such a  $(u_i, t_i)$ . The Riemannian tensor is a collection  $\{R_{i^l jk}^l\}_{i,l,j,k}, 1 \leq i, l, j, k \leq d-1$ , which can be computed as [Millman and Parker, 1977]

$$R_{i^l jk}^l = \frac{\partial}{\partial u^j} \Gamma_{ik}^l - \frac{\partial}{\partial u^k} \Gamma_{ij}^l + \sum_{p=1}^{d-1} (\Gamma_{ik}^p \Gamma_{pj}^l - \Gamma_{ij}^p \Gamma_{pk}^l). \quad (6)$$

Finally, the Ricci tensor is a contraction of the Riemannian tensor, and so

$$\text{Ric}(g(u, t))_{ik} = R_{i^l lk} = \sum_{l=1}^{d-1} R_{i^l lk}, \quad (7)$$

where the term in the middle uses Einstein notation, is the corresponding Ricci tensor at a particular  $(u, t)$ , which is equivalently an analog of the trace of the Riemannian tensor.

### 3 Methodology

We present Ricci flow-guided autoencoders to learn PDE dynamics. From a collection of PDE observations with known initial data with parameter  $\alpha$ , we develop a series of neural networks, first mapping to a parameterization domain, then a manifold encoding, which is then decoded as a prediction to PDE output. An interposed neural network acts as the metric as well as a solution to Ricci flow, in which the relation between the tangent vectors to the manifold and the metric acts as Ricci flow enforcement.

**Neural network design.** Necessary PDE information acts as input training data into a parameterization neural network  $\mathcal{P}_{\theta_{\mathcal{P}}}$ , mapping such data to a point in the parameterization domain  $\mathcal{U}$  of the manifold continuum  $\mathcal{M}_{\hat{\tau}}$ . In particular, we construct a neural network  $\mathcal{P} : \tilde{\Phi} \times \Theta_{\mathcal{P}} \rightarrow \mathcal{U}$ , where  $\tilde{\Phi}$  is an  $N$ -dimensional vector containing data of the PDE initial conditions  $\{\phi_0^i\}_i$ ,  $\phi_0^i = \{(\phi_0^i(x_1, 0), \dots, \phi_0^i(x_N, 0)) : x_j \in \Omega\}$  for mesh  $\Omega$ . We denote  $\mathcal{P}_{\theta_{\mathcal{P}}}(\phi) = \mathcal{P}(\phi, \theta_{\mathcal{P}})$ . The purpose of this neural network, instead of directly mapping PDE information into a manifold latent space, is so that the partial derivatives  $\partial_i \mathcal{E}(u, t)$ , hence tangent vectors, of the manifold may be taken with respect to the same domain in which the metric  $g$  is defined. Without this, 4 cannot be formulated, which invalidates one of the terms we will develop in our loss function.

We propose a physics-informed neural network (PINN) framework for finding the metric solution  $g$  to the Ricci flow equation. The PINN  $g_{\theta_g}$  is constructed via standard neural network architecture, but is substituted into the pertinent PDE and is subsequently minimized as a PDE residual, as this is set to 0 in what should be satisfied [Raissi et al., 2017]. Differentiation of the PINN can be performed using automatic differentiation techniques found in deep learning libraries. To construct the metric, let  $g : \mathcal{U} \times [0, \tau] \times \Theta_g \rightarrow \mathbb{M}^{m \times m}$ , where  $\mathbb{M}^{m \times m}$  is the set of  $m \times m$  matrices. Generally,  $m = d - 1$ . Since the metric should satisfy Ricci flow, the PDE residual to be minimized in our PINN setup is  $\partial_t g_{\theta_g} + 2\text{Ric}(g_{\theta_g})$  [Jain et al., 2022].

Lastly, we construct encoder of decoder networks. The encoder maps a point along the learned parameterization domain directly onto the manifold embedded in Euclidean space at a specified time, and so the encoder additionally has a temporal input parameter corresponding to a state of evolution of the manifold. The encoder is given by  $\mathcal{E} : \mathcal{U} \times [0, \tau] \times \Theta_{\mathcal{E}} \rightarrow \mathcal{M}_{\hat{\tau}}$ , for  $\hat{\tau} \in [0, \tau]$ . The decoder,  $\mathcal{D} : \mathcal{M}_{\hat{\tau}} \times \Theta_{\mathcal{D}} \rightarrow \mathbb{R}$ , maps the point in Euclidean coordinates directly to known PDE solutions. A series of compositions of functions is taken to yield the final autoencoder output, with loss restrictions imposed on the various functions at the intermediate steps to ensure the desired conditions, such as the manifold evolving under Ricci flow, are satisfied.

**Loss function.** We construct our training objective function as follows:

$$\theta = \arg \min_{\theta \in \Theta} \mathcal{L}_{Ric}(\theta) + \lambda_{dec} \mathcal{L}_{dec}(\theta) + \lambda_{met} \mathcal{L}_{met}(\theta) \quad (8)$$

$$\mathcal{L}_{Ric}(\theta) = \mathbb{E}_t \mathbb{E}_{\Phi} \left[ \frac{1}{|\mathcal{U}|^2} \|\partial_t g_{\theta_g}(u, \hat{\tau}) + 2\text{Ric}(g_{\theta_g}(u, \hat{\tau}))\|_F^2 \right] \quad (9)$$

$$\mathcal{L}_{dec}(\theta) = \mathbb{E}_t \mathbb{E}_{\Phi} \left[ \frac{1}{N} \sum_j |\mathcal{D}_{\theta_{\mathcal{D}}, j}(\mathcal{E}_{\theta_{\mathcal{E}}}(u, \hat{\tau})) - \phi_j|^2 \right], \quad (10)$$

$$\mathcal{L}_{met}(\theta) = \mathbb{E}_t \mathbb{E}_{\Phi} \left[ \frac{1}{|\mathcal{U}|^2} \|g_{\theta_g}(u, \hat{\tau}) - (J\mathcal{E}_{\theta_{\mathcal{E}}}(u, \hat{\tau}))^T (J\mathcal{E}_{\theta_{\mathcal{E}}}(u, \hat{\tau}))\|_F^2 \right], \quad (11)$$

where we use notation  $J\mathcal{E}_{\theta_{\mathcal{E}}}$  to denote the Jacobian of vector  $\mathcal{E}_{\theta_{\mathcal{E}}}$  with respect to  $u$ , i.e.

$(J\mathcal{E}_{\theta_\varepsilon}(u, \hat{\tau}))^T(J\mathcal{E}_{\theta_\varepsilon}(u, \hat{\tau}))$  is the matrix of inner products

$$(J\mathcal{E}_{\theta_\varepsilon}(u, \hat{\tau}))^T(J\mathcal{E}_{\theta_\varepsilon}(u, \hat{\tau})) \quad (12)$$

$$= \begin{pmatrix} \|\partial_1\mathcal{E}_{\theta_\varepsilon}(u, \hat{\tau})\|_2^2 & \langle\partial_1\mathcal{E}_{\theta_\varepsilon}(u, \hat{\tau}), \partial_2\mathcal{E}_{\theta_\varepsilon}(u, \hat{\tau})\rangle & \dots \\ \langle\partial_2\mathcal{E}_{\theta_\varepsilon}(u, \hat{\tau}), \partial_1\mathcal{E}_{\theta_\varepsilon}(u, \hat{\tau})\rangle & \|\partial_2\mathcal{E}_{\theta_\varepsilon}(u, \hat{\tau})\|_2^2 & \dots \\ \vdots & \vdots & \ddots \end{pmatrix}. \quad (13)$$

We motivate our loss so that the relation between the metric and the inner product of derivatives of 4 is satisfied under Ricci flow. A difference between decoder prediction and PDE solution is minimized to ensure a proper output.

The first expectation runs over time, and the second runs over training data, taking data  $\phi_0^i \sim \Phi$  for PDE data belonging to distribution  $\Phi$ . We use notation  $|\mathcal{U}| = \dim(\mathcal{U})$ . Denote  $\{u_i\}_i, u_i = \mathcal{P}_{\theta_{\mathcal{P}}}(\phi_0^i)$ , an enumeration of values within  $\mathcal{U}$ , which are learned via neural network  $\mathcal{P}_{\theta_{\mathcal{P}}}$  and not set beforehand, corresponding to points in the training data. Denote  $\{\phi_j^i\}_{j,i}, \phi_j^i(\cdot, t^*) = \{\phi^i(x_j, t^*) : x_j \in \Omega, t^* \in [0, T]\}$ , an enumeration of output training data. Denote  $\mathcal{D}_{\theta_{\mathcal{D}},j}(\cdot)$  the  $j$ -th element of the output of  $\mathcal{D}_{\theta_{\mathcal{D}}}$ . Let  $\Theta = (\Theta_{\mathcal{P}}, \Theta_g, \Theta_{\mathcal{E}}, \Theta_{\mathcal{D}})$ . Let  $\hat{\tau} \in U([0, \tau]), \tilde{\tau} \in U([0, \tau'])$  be uniformly sampled via a collocation procedure, where  $\tau = CT$  for some constant  $C$ , and  $\hat{\tau}$  and  $\tilde{\tau}$  are times associated with each other by some linear scaling. We will generally choose  $\hat{\tau} = \tilde{\tau}$ . We scale the times belonging to Ricci flow  $\hat{\tau}$ , primarily to ensure no singularities develop, which are possible under an identity relationship.  $\|\cdot\|_F$  is the Frobenius norm. All derivatives are computed via automatic differentiation found in standard deep learning libraries. The analytic expectations can be taken using empirical averages during the training procedure, additionally divided into batches with parameters updated with a stochastic optimizer.

The loss terms are organized as a Ricci flow physics-informed term  $\mathcal{L}_{Ric}$ , quadratic loss  $\mathcal{L}_{dec}$  to ensure the decoder matches the PDE solution, and a constraint term  $\mathcal{L}_{met}$  to match the manifold evolution with the metric satisfying Ricci flow.  $\lambda_{dec}$  and  $\lambda_{met}$  are scaling coefficients as needed. In the final term  $\mathcal{L}_{met}$ ,  $g_{\theta_g}$  is the matrix of the physics-informed metric term  $g_{\theta_g}$ , where the components are summed with respect to each inner product  $\langle\partial_j\mathcal{E}_{\theta_\varepsilon}(u_i), \partial_k\mathcal{E}_{\theta_\varepsilon}\rangle$  to enforce loss for each entry.

We will generally restrict our attention to the case  $\mathcal{U} \subseteq \mathbb{R}^2$ . as this exhibits computational simplicity in the training procedure, yet sufficient latent representation.  $\mathcal{U}$  generally parameterizes a 2-dimensional manifold, i.e.  $\mathcal{E}(u, t)$  is embedded in  $\mathbb{R}^3$ .

**Special cases.** Special cases of Ricci flow may be under consideration, which are favorable for reasons such as lower computational cost or higher-dimensional encodings. In these scenarios, information about the manifold is set beforehand, such as the metric. Ideal latent geometries are sacrificed at the gain of some other benefit. We discuss special cases in Appendix D. Coordinate transformations may be appropriate under select special cases. Our method in such a setting is discussed in Appendix C.

## 4 Experiments

We present Ricci flow-guided autoencoders on a series of numerical experiments for approximate solutions of PDEs given collections of known data. We compare our method to existing GD-variational autoencoder methods in [Lopez and Atzberger, 2022], as well as other forms of autoencoder baselines. Results for both the Ricci flow method and alternative methods are collected using identical initial condition input spaces. The GD-VAE method is performed using an evolution mapping  $\phi_t \rightarrow \phi_{t+\tilde{t}}$ , where  $\tilde{t}$  is some time-increment used to progress the solution to a later time. Predictions are retrained for new values of  $\tilde{t}$ .

---

**Algorithm 1** Training algorithm of Ricci flow-guided autoencoders

---

**Input:** Initial conditions  $\{\phi_0^i\}_i$ , solutions  $\{\phi_{t_j}^i\}_{i,j}$  evaluated at  $(\cdot, t_j) \in \Omega \times [0, T]$

**Setup:** Set  $\hat{\tau}_i = C_t t_i$ , sample  $\tilde{\tau}_i \in U([0, \tau])$  for some final  $\tau$ . Select batch size  $n$

- 1: **while**  $\mathcal{L}(\theta)$  is not converged **do**
  - 2:   Sample  $n$  initial conditions  $\{\phi_0^i\}_{i \in \mathcal{I}_n}$  and  $n$  solutions  $\{\phi_{t_j}^i\}_{i \in \mathcal{I}_n, j \in \mathcal{J}_n}$
  - 3:    $u_i = \mathcal{P}_{\theta_{\mathcal{P}}}(\phi_0^i) \in \mathcal{U}$
  - 4:   Compute encoded point on manifold  $\mathcal{E}_{\theta_{\mathcal{E}}}(u_i, \hat{\tau}_i)$
  - 5:   Compute decoded solution  $\mathcal{D}_{\theta_{\mathcal{D}}}(\mathcal{E}_{\theta_{\mathcal{E}}}(u_i, \hat{\tau}_i))$
- 

**Ricci flow loss**

---

Compute:

- 6:    $\partial_t g_{\theta_g}(u_i, \tilde{\tau}_i)$  ▷ time derivative
  - 7:    $g^{kl} \in G^{-1}$  ▷ inverse matrix of metric
  - 8:    $\partial_i g_{jk}$  ▷ partial derivatives
  - 9:    $\partial_{il} g_{jk}$  ▷ second order partial derivatives
  - 10:    $\Gamma_{ij}^l = \frac{1}{2} \sum_k g^{kl} (\partial_j g_{ik} - \partial_k g_{ij} + \partial_j g_{kj})$  ▷ Christoffel symbols
  - 11:    $R_{i\ jk}^l = \partial_j \Gamma_{ik}^l - \partial_k \Gamma_{ij}^l + \sum_p (\Gamma_{ik}^p \Gamma_{pj}^l - \Gamma_{ij}^p \Gamma_{pk}^l)$  ▷ Riemannian tensor
  - 12:    $\text{Ric}(g(u, t))_{ik} = \sum_l R_{i\ lk}^l$  ▷ Ricci tensor
  - 13:   Loss  $\mathcal{L}_{Ric}(\theta)$
- 

**Metric loss**

---

- 14:   Compute  $\langle \partial_j \mathcal{E}_{\theta_{\mathcal{E}}}(u_i, \hat{\tau}_i), \partial_k \mathcal{E}_{\theta_{\mathcal{E}}}(u_i, \hat{\tau}_i) \rangle$  ▷ inner product constraint
  - 15:   Formulate  $\mathcal{L}_{met}(\theta)$  from above and physics-informed metric  $g_{\theta_g}$
- 

**Decoder loss**

---

- 16:   Compute  $\mathcal{L}_{dec}(\theta)$  directly from decoder and  $\{\phi^i(\cdot, t_j)\}$
- 

**Minimize objective.**

---

- 17:   Compute  $\mathcal{L}_{Ric}(\theta) + \lambda_{dec} \mathcal{L}_{dec}(\theta) + \lambda_{met} \mathcal{L}_{met}(\theta)$
  - 18:   Update  $\theta$
  - 19: **end while**
- 

The highlighting feature of our method is the manifold latent space subject to Ricci flow. We will reserve comparisons for recreating data as seen as part of the training procedure for manifold-based methodology to emphasize results for such a variety of framework.

## 4.1 Viscous Burger’s equation

1-d Burger’s equation					
method	$t = 0$	$t = 0.25$	$t = 0.5$	$t = 0.75$	$t = 1$
Ricci flow	$1.76 \pm 1.38$	$1.53 \pm 0.502$	$1.43 \pm 0.586$	$1.38 \pm 0.740$	$2.19 \pm 0.970$
GD-VAE	-	$14.4 \pm 18.9$	$4.52 \pm 5.47$	$4.90 \pm 6.88$	$3.75 \pm 3.68$
AE, g-proj.	-	$10.3 \pm 10.6$	$10.4 \pm 7.89$	$5.29 \pm 11.9$	$2.24 \pm 1.13$

Table 1: We compare our methodology to those existing, reporting relative  $L^1$  errors on 30 testing sets. All errors are taken  $10^{-2}$ . Times corresponding to the increment  $\tilde{t} = 0$  are omitted for comparisons since this is a trivial learning task in these frameworks.

We first introduce our method on the viscous Burger’s equation. The viscous Burger’s equation is given by

$$\partial_t \phi(x, t) + \phi(x, t) \partial_x \phi(x, t) = \nu \partial_x^2 \phi(x, t), \quad (14)$$

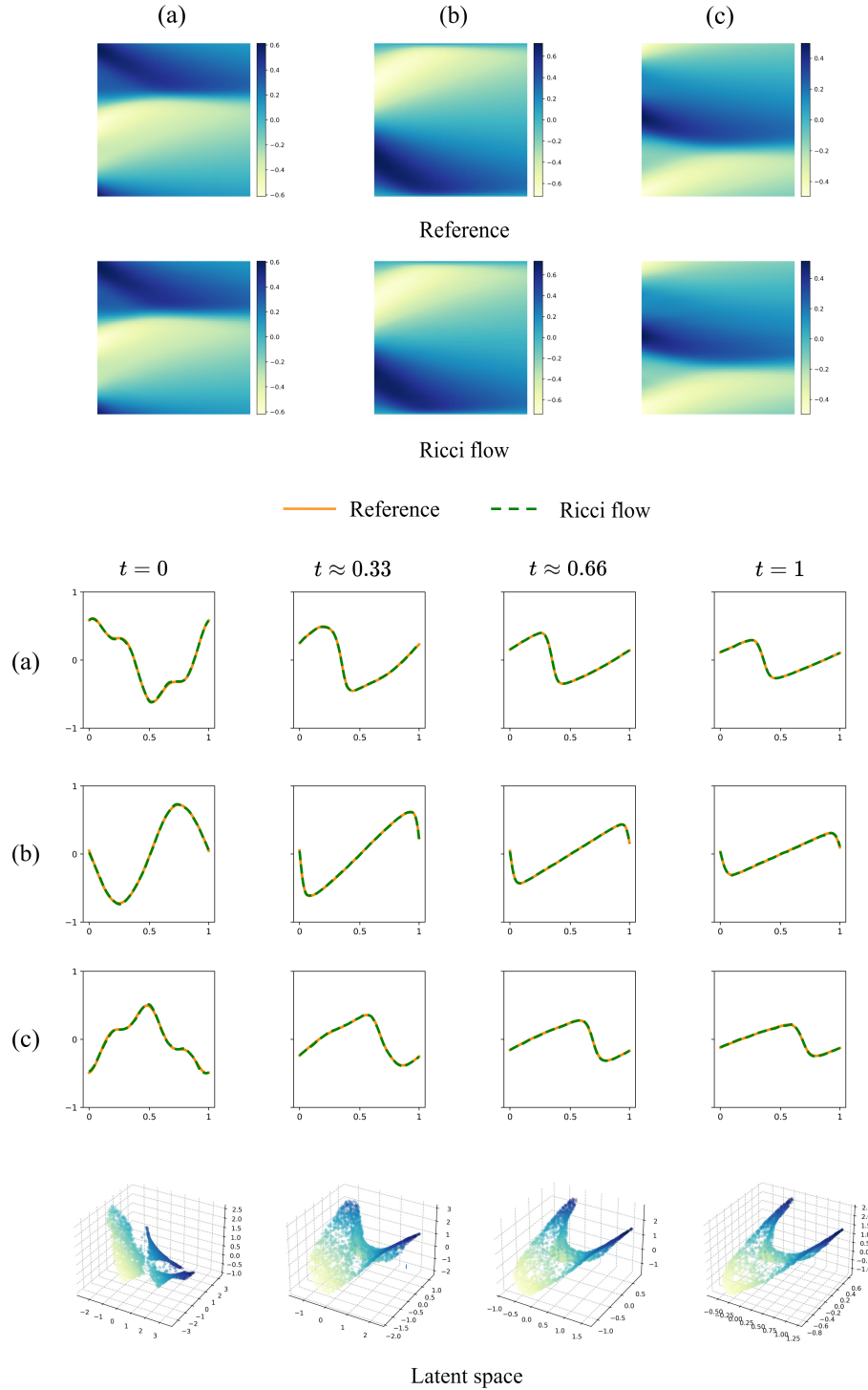


Figure 1: Illustration of numerical Burger's equation solutions versus their Ricci flow solutions, as well as the manifold latent space over all training data. (a)-(c) represent three distinct solutions, with the top images being the solutions conveyed in 2-d with time versus 1-d space, while the middle images are cross sections of the top with respect to space at selected times. The evolving latent space is given at such times at the bottom.

for diffusion coefficient parameter  $\nu \in \mathbb{R}$  [Lopez and Atzberger, 2022].

Our numerical evaluations for training and test data were constructed using a psuedo-spectral method with Fast Fourier transforms [Binder, 2021b]. Evaluations were over a  $(x, t) \in [0, 1] \times [0, 1]$  domain discretized into an equispaced grid  $\Omega_x \times \Omega_t$  with mesh distance  $h_x = h_t = 0.01$ . Kinematic viscosity coefficient  $\nu = 0.01$  was chosen. Initial conditions were evaluated from  $\mathcal{A}_1 = \{\phi_0 : \phi_0 = \phi(x, 0) = \alpha \sin(2\pi x) + \beta \cos^3(2\pi x), \alpha, \beta \in [-1, 1]\}$ . We choose training data by uniformly sampling 100 of  $\phi_t$  for  $t \in \Omega_t$  per each  $\phi_0$ .

1-d Burger's extrapolation	
method	$\mathcal{A}_1^{new}, t = 0.35$
Ricci flow	$17.2 \pm 14.2$
GD-VAE	$36.1 \pm 17.8$
AE	$24.7 \pm 20.3$

Table 2: We examine relative  $L^1$  error for out-of-distribution data.

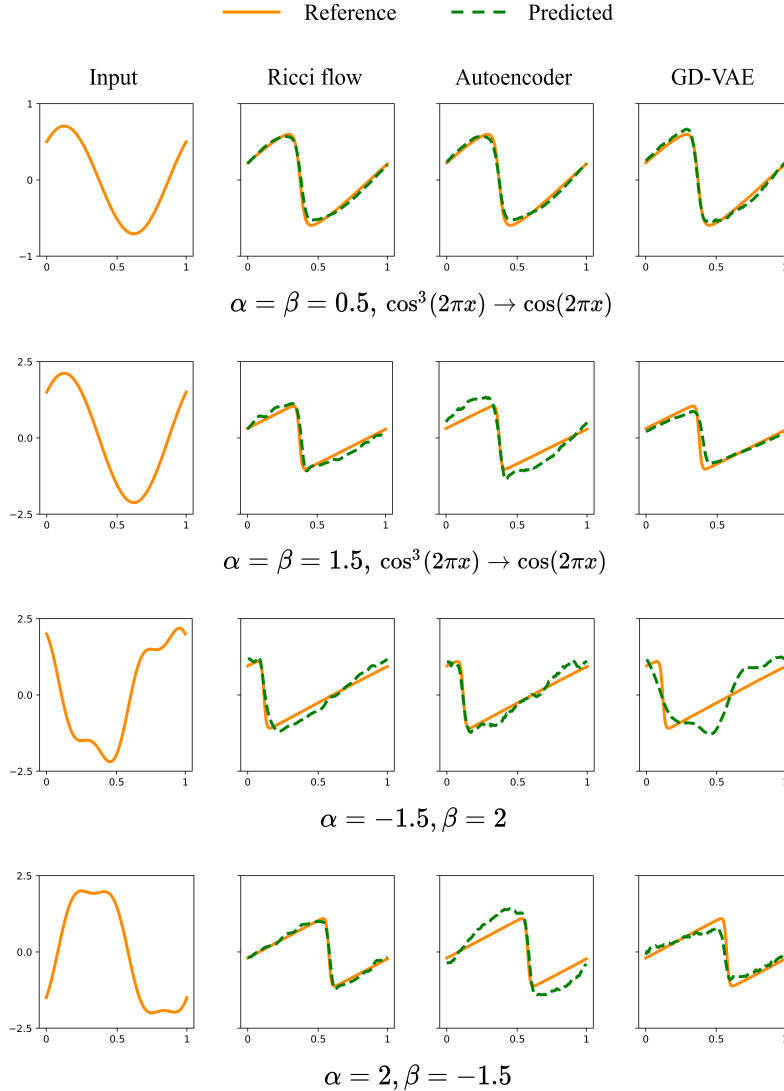


Figure 2: We compare various methodology in the extrapolation setting of out-of-distribution input data of varying difficulty for Burger's equation. We examine  $t = 0.35$ .

Training consisted of a generation of 3,000 initial conditions. Loss coefficients  $\lambda_{dec} = \lambda_{met} = 1$  were taken. We found training to occasionally be unstable, individuated by sudden increases in loss by orders of magnitude, resolvable by using a low learning rate, weight decay, and gradient clipping. The weight decay parameter was reduced in late training to ensure satisfaction of the objective.

Architecture consisted of relative modesty in regard to capacity. Width of  $w = 120$  was chosen for all neural networks in this experiment, which exhibited a balance of sufficiency and simplicity. All neural networks held 3 hidden layers. Experimentation for activation was upon both  $\text{GELU}(\cdot)$  and  $\text{tanh}(\cdot)$ , a choice of which was nonvital for success; however, we remark activation with sufficient continuous differentiability properties are necessary, as second order derivatives are taken to formulate the physics-informed Ricci flow, and activation such as  $\text{ReLU}(\cdot)$  has second derivative 0 almost everywhere.

We examine our methodology on out-of-distribution cases belonging to the same family of data as training data, but for parameter specifications that deviate from those used in training. In Figure 2, we give a comparison of our methodology, listing the changes made to the data. We list extrapolation error results in Table 2. Our extrapolation baselines are the GD-VAE framework, and a vanilla autoencoder with hyperparameters matching that of the Ricci flow setting when applicable, including a latent space of  $\mathbb{R}^3$ . The AE g-proj. autoencoder as presented in [Lopez and Atzberger, 2022] is the autoencoder baseline in the in-distribution test setting, maintaining consistency between manifold-based methods for in-distribution cases.

## 4.2 Diffusion-reaction equation

In this experiment, we study the setting of the 1-dimensional diffusion-reaction PDE with source term, given by the equation [Wang et al., 2021]

$$\partial_t \phi(x, t) = D \partial_x^2 \phi(x, t) + \lambda \phi^2(x, t) + f(x), \quad (15)$$

for diffusion coefficient  $D \in \mathbb{R}$ , reaction rate  $\lambda \in \mathbb{R}$ , and source term  $f$ .

Our numerical scheme for constructing data was a finite difference solver [Wang et al., 2021]. Datasets were constructed over a  $(x, t) \in [0, 1] \times [0, 1]$  domain. We choose mesh distance  $h_x = h_t = 0.01$ . We generated initial data from  $f(x)$ , using a special case of a Fourier series,  $\mathcal{A}_2 = \{f : f(x) = \alpha \sin(2\pi x) + \frac{\alpha+0.5}{2} \cos(4\pi x) + \frac{\beta}{3} \sin(4\pi x), \alpha, \beta \in [-1, 1]\}$ . The sum taken in the second coefficient ensures non-triviality of the initial data. Training data is normalized so that  $\int_{\mathcal{X}} \phi_0 dx = 1$ , and the same scaling coefficient also scales data at time  $t > 0$ . We learn the mapping  $(\phi_0, t) \rightarrow \phi_t$  despite initial functions being sampled for  $f$  and not  $\phi_0$ .

1-d diffusion-reaction					
	$t = 0$	$t = 0.25$	$t = 0.5$	$t = 0.75$	$t = 0.9$
Ricci flow	$0.274 \pm 0.136$	$0.184 \pm 0.0755$	$0.215 \pm 0.0932$	$0.429 \pm 0.199$	$1.14 \pm 0.410$
GD-VAE	-	$2.10 \pm 2.81$	$2.94 \pm 6.17$	$1.53 \pm 0.886$	$2.24 \pm 0.881$
AE, g-proj.	-	$1.78 \pm 2.59$	$1.28 \pm 0.903$	$1.41 \pm 0.595$	$2.77 \pm 1.33$

Table 3: We compare  $L^1$  errors in methodology for the diffusion-reaction experiment on in-distribution data. All values are taken  $10^{-2}$ . We see our method achieves about one order of magnitude lower than baseline methods. While our method achieves competitive error even with vanilla architecture, such a decrease by an order of magnitude is partially attributed to the modified MLP augmented architecture.

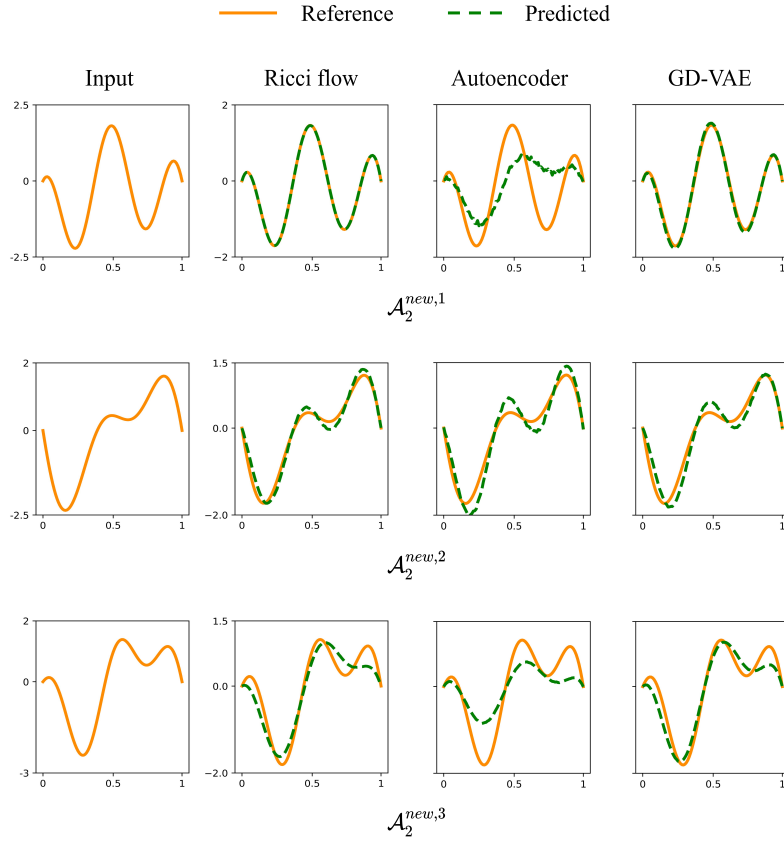


Figure 3: We compare various methodology in the extrapolation setting for the diffusion-reaction equation. We examine  $t=0.35$ .

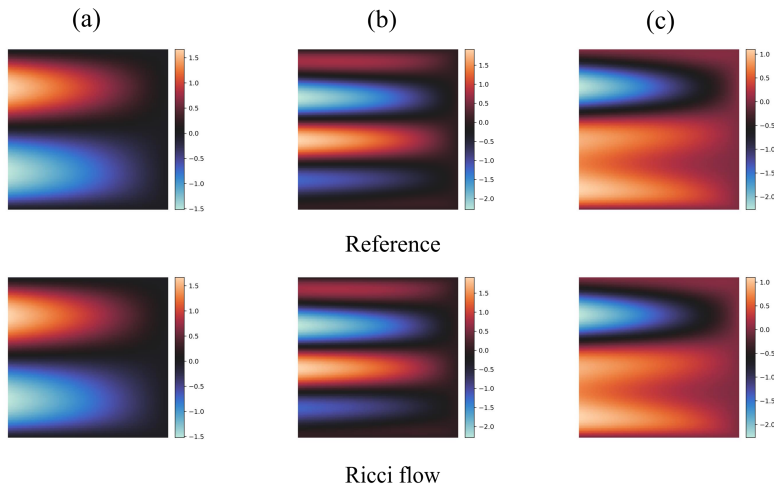


Figure 4: Illustration of numerical diffusion-reaction equation solutions versus their Ricci flow solutions. (a)-(c) represent three distinct solutions.

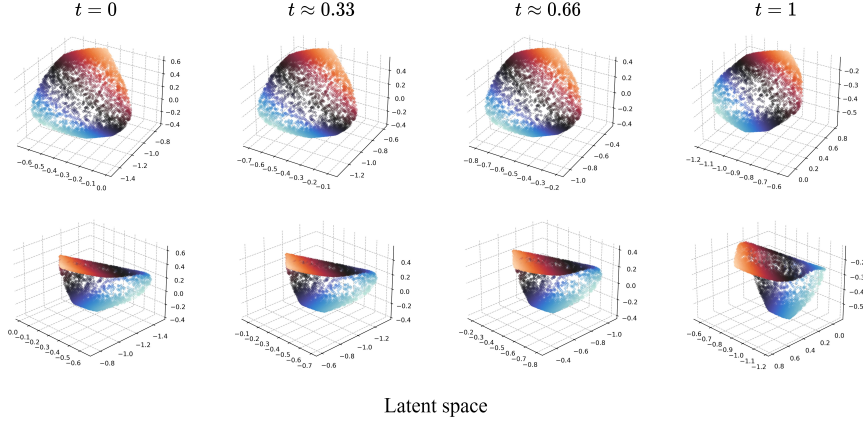


Figure 5: Illustration of the manifold latent space subject to Ricci flow in learning diffusion-reaction PDE data from varying angles.

1-d diffusion-reaction extrapolation			
	$\mathcal{A}_2^{new,1}, t = 0.35$	$\mathcal{A}_2^{new,2}, t = 0.35$	$\mathcal{A}_2^{new,3}, t = 0.35$
Ricci flow	$10.4 \pm 15.4$	$17.8 \pm 9.62$	$30.8 \pm 13.1$
GD-VAE	$14.9 \pm 17.0$	$21.9 \pm 13.9$	$36.1 \pm 18.6$
AE	$19.4 \pm 27.0$	$23.6 \pm 12.8$	$47.5 \pm 26.3$

Table 4: We compare  $L^1$  errors in methodology for the diffusion-reaction experiment on extrapolation data. All values are taken  $10^{-2}$ .

We implement an augmented architecture, the modified multilayer perceptron (MMLP), in this experiment, which has demonstrated success in physics-informed settings [Wang et al., 2021]. This architecture is elaborated upon in Appendix F, with training loss illustrated in Appendix 9, indicating this architecture achieves an order of magnitude lower training loss in fewer iterations of the Adam optimizer. In Table 4.2, our autoencoder baseline in the extrapolation setting uses the architecture used in the Ricci flow setting to allow fair comparison despite the baseline autoencoder being a non-physics-informed setting.

Training consisted of 5,000 samples from  $A_2$  paired with 100 uniformly sampled evaluations at later times  $\phi_0(\cdot, t^*)$ . Architecture consisted of 5 hidden layers for each network, a hidden layer being the term  $\zeta^i$  as illustrated in Appendix F, which had a width of 100. GELU( $\cdot$ ) was used for all activations.

We reduced the latent dimension of the autoencoder baseline used in the extrapolation table of Table 4.2 to  $d = 2$ , but the autoencoder failed to learn and solve the objective function sufficiently well. The reason this was done as our Ricci flow method has  $\mathcal{U} \subseteq \mathbb{R}^2$ , but the inability to learn is not observed in our method. The autoencoder latent dimension  $\mathbb{R}^3$  is most applicable for comparison, which is indeed the space in which our manifold is embedded under Ricci flow in this experiment.

### 4.3 Navier-Stokes equation

We test our method on the 2-d incompressible Navier-Stokes equation, [Crews, 2021]

$$\partial_t v(x, t) + (v(x, t) \cdot \nabla)v(x, t) - \nu \nabla^2 v(x, t) = \frac{-1}{\rho} \nabla p(x, t), \quad (16)$$

given by the velocity field  $v$  evolution subject to the constraint  $\nabla \cdot v = 0$ , which is the incompressibility condition, and given an initial velocity vector field  $v_0$  and pressure field over grid  $\Omega_x \subseteq \mathcal{X} \subset \mathbb{R}^2$ . The vorticity  $\phi = \nabla \times v$  serves as training data, where  $\nabla \times$  denotes the curl. We learn the autoencoder mapping  $[(\nabla \times v_0)]_z \times t \rightarrow \phi_t$ , where  $[\cdot]_z$  is the  $z$ -th coordinate over  $\Omega_x$ . Data for this experiment was constructed using a discontinuous Galerkin/Fourier spectral solver [Crews, 2021].

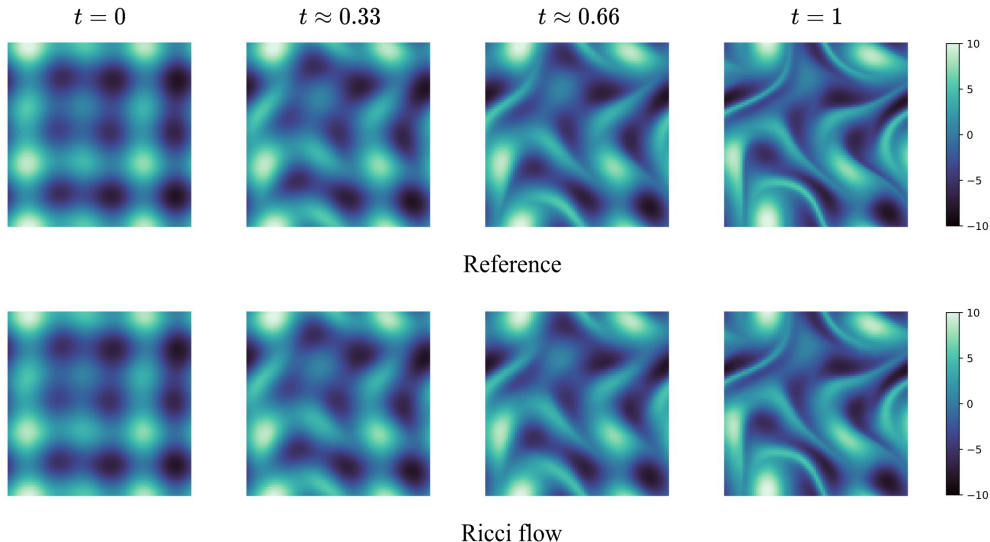


Figure 6: Comparison of numerical solution to our Ricci flow solution in the test setting on Navier-Stokes solution data.

2-d Navier-stokes equation					
	$t = 0$	$t = 0.25$	$t = 0.5$	$t = 0.75$	$t = 1.0$
Ricci flow	$4.44 \pm 1.48$	$3.97 \pm 1.57$	$5.26 \pm 1.18$	$8.46 \pm 1.09$	$9.25 \pm 1.53$
GD-VAE	-	$84.3 \pm 8.92$	$88.4 \pm 12.8$	$93.5 \pm 5.05$	$92.1 \pm 4.02$

Table 5: We demonstrate methodology on the Navier-Stokes experiment. In practice, we found the GD-VAE framework altogether unsuitable for this experiment.

We consider the special case of Ricci flow upon the  $(n - 1)$ -sphere. Data for this experiment consisted of  $80 \times 80$  meshes in  $\mathbb{R}^2$ , data of markedly higher dimensionality than in the previous experiments. A parameterization representation in  $\mathbb{R}^2$  and an embedding in  $\mathbb{R}^3$  were empirically found to be too modest in dimensionality to thoroughly encapsulate the data, and information was lost through such compression to accurately reconstruct solutions as well as provide prediction capacity. An encoding onto the  $(n - 1)$ -sphere allows for a dimension increase in  $\mathcal{U}$  and the embedding space  $\mathbb{R}^d$  by a reduction in the numerical power needed. While the manifold still evolves under a closed form of Ricci flow, the fixed geometries do not harmonize with the PDE data as well as other geometries learned via training, but the latent expressivity is significant enough to make the evolving  $(n - 1)$ -sphere preferable for a manifold.

A convolutional neural network (CNN) was used for the parameterization network  $\mathcal{P}_{\theta_P}$ , taking 2-d grid input and mapping to  $\mathcal{U} \subseteq \mathbb{R}^{100}$  for manifold parameterization. The

$(n - 1)$ -sphere was embedded in  $\mathbb{R}^{101}$ . We observed an artificial neural network gained greater empirical success over a deconvolutional neural network, or a CNN with transpose layers, for the decoder, achieving lower training error in fewer iterations of the Adam optimizer. Architecture for the decoder was taken as 101 – 400 – 1600 – 6400 – 6400 – (output), an architecture susceptible to overfitting. We applied techniques to prevent such, as described below. Wide architecture with severe overfitting regularization gained empirical favor over narrow architecture with modest regularization in the test setting.

Overfitting techniques were conducive towards generalization and accurately reconstructing solutions in the test setting. These techniques were notably dropout and adding Gaussian noise to the intermediate steps in producing the output, such as the parameterization space and the manifold in the embedded space [Amir, 2020]. Dropout was only used in the decoder, set in earlier layers as  $p = 0.35$  and reduced before the final layer to  $p = 0.25$ . For the Gaussian noise, we first took a parameterization output  $u \in \mathcal{U}$  and recast it as  $u + C_{\xi^u} \cdot u \odot \xi^u$ , where we use  $[\xi^u]_{ij} \sim \mathcal{N}(0, 1)$  to denote a tensor with standard normal elements  $[\cdot]_{ij}$  with the same dimensions as  $u$ .  $C_{\xi^u}$  denotes a scaling constant, which we took as 0.035. The element-wise multiplication with  $u$  ensures the Gaussian noise scales with  $u$  to prevent imbalance. Gaussian noise was then added to manifold of the form  $\mathcal{M} + C_{\xi^{\mathcal{M}}} \cdot r(\tau) \cdot \xi^{\mathcal{M}}$ , instead scaling with the radius here and denoting  $\Phi^{\mathcal{M}}$  the analog of  $\xi^u$  for the manifold. We chose  $C_{\xi^{\mathcal{M}}} = 0.075$ .

Training data generation was costly for this experiment, taking about  $\sim 8$  hours to generate 2200 solutions, 2000 for training and 200 for test. Such an increase in data is a less-viable option to reduce overfitting, which may also be a limited option in practice.

The GD-VAE framework was established for this experiment using the baseline architecture as presented, but width and depth were expanded to accommodate the increased difficulty of learning the data. Deep artificial neural networks were used for both the encoder and decoder. In practice, this methodology without heavy modification presented itself as unsuitable for this experiment, potentially due to latent dimensionality.

## 5 Future work and limitations

Extrapolation data seems to cohere to some structure as developed by the manifold and the Ricci flow, as observable by the figures in Appendix H. While our method demonstrates empirical favor in extrapolation, additional work could be created that seeks a method to incorporate extrapolation data into the manifold in a more effective way while simultaneously allowing an implicitly-learned manifold via neural network subject to a geometric flow, which could in turn improve extrapolation results even further.

[Lopez and Atzberger, 2022] notes certain qualities such as periodicity work together with certain latent geometries. While optimality of geometry can be empirically observed, especially from an error analysis perspective, the concept of optimality of geometry could be further analyzed from a theoretical perspective, especially from a deep learning theory perspective. One may attempt to quantify the question: how do deep neural networks harmonize well with data in a sense of geometry, particularly a geometric latent space? This topic could be explored, in which one may incorporate results into the methodology as seen here.

## 6 Acknowledgments

We would like to thank Xiaohui Chen for helpful discussions in developing this project, particularly regarding intrinsic versus extrinsic geometric flows.

## References

- Amir. Answer to "adding random noise to latent representation increase the accuracy in the autoencoder". licensed under cc by-sa 3.0, 2020. URL <https://stats.stackexchange.com/questions/452267/adding-random-noise-to-latent-representation-increase-the-accuracy-in-the-autoen>.
- Arapura. M462 (handout 9). URL <https://www.math.purdue.edu/~arapura/preprints/diffgeom9.pdf>.
- Sacha Binder. Wave equation simulations 1d/2d (équation de d'alembert), 2021a. URL [https://github.com/sachabinder/wave\\_equation\\_simulations](https://github.com/sachabinder/wave_equation_simulations).
- Sacha Binder. Burgers' equation simulation 1d (simulation de l'équation de burgers), 2021b. URL [https://github.com/sachabinder/Burgers\\_equation\\_simulation/tree/main](https://github.com/sachabinder/Burgers_equation_simulation/tree/main).
- Danny Calegari. Chapter 7: Ricci flow, 2023. URL [https://math.uchicago.edu/~dannyc/courses/ricci\\_2019/ricci\\_flow.pdf](https://math.uchicago.edu/~dannyc/courses/ricci_2019/ricci_flow.pdf).
- Daniel W. Crews. Incompressible2d, 2021. URL <https://github.com/crewsdw/Incompressible2D>.
- hft. Answer to "tensor contraction criteria". licensed under cc by-sa 3.0, 2023. URL <https://physics.stackexchange.com/questions/743533/tensor-contraction-criteria>.
- Olivier Hénot. The ricci flow equation, 2019. URL [https://www.math.mcgill.ca/gantumur/math581w19/ricci\\_flow\\_olivier.pdf](https://www.math.mcgill.ca/gantumur/math581w19/ricci_flow_olivier.pdf).
- Aarjav Jain, Challenger Mishra, and Pietro Liò. A physics-informed search for metric solutions to ricci flow, their embeddings, and visualisation, 2022.
- Yangyang Li and Ruqian Lu. Applying ricci flow to high dimensional manifold learning, 2017.
- Ryan Lopez and Paul J. Atzberger. Gd-vaes: Geometric dynamic variational autoencoders for learning nonlinear dynamics and dimension reductions, 2022.
- Richard S. Millman and George D. Parker. *Elements of Differential Geometry*. Prentice Hall, Inc., Englewood Cliffs, New Jersey 07632, 1977.
- orangesoda. Answer to "what is the metric tensor on the n-sphere (hypersphere)?" . licensed under cc by-sa 3.0, 2013. URL <https://math.stackexchange.com/questions/402102/what-is-the-metric-tensor-on-the-n-sphere-hypersphere>.
- Maziar Raissi, Paris Perdikaris, and George Em Karniadakis. Physics informed deep learning (part i): Data-driven solutions of nonlinear partial differential equations, 2017.
- Nick Sheridan. Hamilton's ricci flow, 2006. URL <https://web.math.princeton.edu/~nsher/ricciflow.pdf>.
- Sifan Wang, Hanwen Wang, and Paris Perdikaris. Learning the solution operator of parametric partial differential equations with physics-informed deepnets, 2021.

## A Extrapolation sets for diffusion-reaction

We list the extrapolation sets used in the diffusion-reaction experiment. They are as follows:

$$\mathcal{A}_2^{new,1} = \{\alpha \sin(2\pi x) + (\gamma + 0.5) \cos(4\pi x) + \beta \sin(4\pi x) : \quad (17)$$

$$\alpha, \beta \in [-1.75, 1.75], \gamma \in [-1, 1]\}, \quad (18)$$

$$\mathcal{A}_2^{new,2} = \{\alpha \sin(2\pi x) + \frac{\alpha + 0.5}{2} \cos(\frac{7}{2}\pi x) + \frac{\beta}{3} \sin(\frac{7}{2}\pi x) : \alpha, \beta \in [0, 1]\}, \quad (19)$$

$$\mathcal{A}_2^{new,3} = \{\alpha \sin(2\pi x) + \frac{\alpha + 1}{2} \cos(\frac{9}{2}\pi x) + \frac{\beta}{3} \sin(\frac{9}{2}\pi x) : \alpha, \beta \in [0, 1]\}. \quad (20)$$

Data is normalized by  $C = \int_{\mathcal{X}} \phi_0 dx$  and scaled by  $C$  for all  $t \in [0, 1]$ .

## B 2-d wave equation experiment

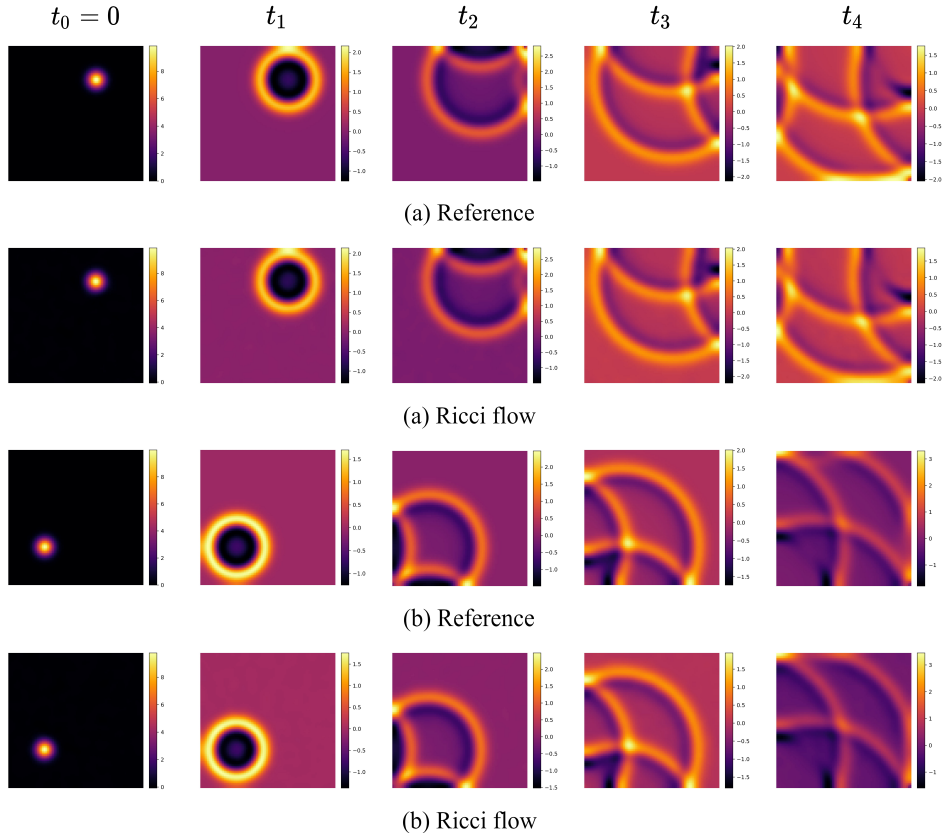


Figure 7: Comparison of numerical solution to our Ricci flow solution in the test setting. (a) and (b) represent two unique solutions.

As a supplemental experiment, we employ our Ricci flow-based method on learning the 2-d wave equation. A finite difference numerical scheme was used for constructing datasets for evaluation [Binder, 2021a]. Neumann boundary conditions were used. A domain  $\mathcal{X} = [0, 5] \times [0, 5]$  was used for space, with time in  $[0, 4]$ . Initial conditions were generated

using a random Gaussian impulse of the form  $\phi_0 = 10 \exp\left\{-\frac{(x-\mu_1)^2}{0.1} - \frac{(y-\mu_2)^2}{0.1}\right\}$ , where  $(\mu_1, \mu_2) \in U([1, 4] \times [1, 4])$  is uniformly random. 1,000 initial condition samples were used with 100 times taken for each initial sample for a training dataset of  $1,000 \times 100 = 100,000$  solutions.

Training details were similar to that of the Navier-Stokes experiment of section 4.3. A convolutional neural network is taken for  $\mathcal{P}_{\theta_{\mathcal{P}}}$ , mapping to  $\mathcal{U} \subseteq \mathbb{R}^{100}$ . The embedding is in  $\mathbb{R}^{101}$ . The special case of Ricci flow along the  $(d-1)$ -sphere is employed. Unlike the Navier-Stokes experiment, overfitting techniques were unnecessary to achieve low empirical error in the test setting, where test data lies from the same underlying distribution as that of training. In particular, injections of noise into various stages of the neural network composition, and dropout, were not needed to achieve generalization in the testing phase. As with the Navier-Stokes experiment, a deep artificial neural network had drastic performance gains over a deconvolutional neural network, taking an architecture of  $101 - 400 - 1600 - 4600 - 4600 - (\text{output})$ , where output is a  $80 \times 80$  mesh of the PDE solution. The final output vector is flattened to yield the desired grid.

## C Coordinate transformations

It may be of interest to transform the base coordinate system for special case extensions. Let  $(u^1, \dots, u^{m_u}) \rightarrow (v^1, \dots, v^{m_v}) : \mathcal{U} \rightarrow \mathcal{V}$  be a coordinate transformation from parameterization domains  $\mathcal{U}$  to  $\mathcal{V}$ . The Christoffel symbols indeed have a closed form under a coordinate transformation, but in order to evaluate Ricci flow in the  $\mathcal{V}$  based on the coordinates of  $\mathcal{U}$ , one only need consider the metric  $g$  and Ricci tensor  $\text{Ric}(g)$ . Denote  $\tilde{g}_{\alpha\beta}$  the metric coefficients under  $\mathcal{V}$ . The metric under this coordinate transformation is [Millman and Parker, 1977]

$$\tilde{g}_{\alpha\beta} = \sum_i \sum_j g_{ij} \frac{\partial u^i}{\partial v^\alpha} \frac{\partial u^j}{\partial v^\beta}, \quad (21)$$

again exchanging the Einstein notation with summation notation. Denote  $\widetilde{\text{Ric}}_{\alpha\beta}(g)$  the Ricci tensor in  $\mathcal{V}$ , and  $\tilde{R}$  the Riemannian tensor in  $\mathcal{V}$ . We will deduce the Ricci tensor under  $\mathcal{V}$  from the Riemannian tensor, which has a known form under a coordinate transformation [Millman and Parker, 1977]

$$\tilde{R}_{\alpha \beta \gamma}^{\delta} = \sum_{i,l,j,k} R_{i \ jk}^l \frac{\partial u^i}{\partial v^\alpha} \frac{\partial v^\delta}{\partial u^l} \frac{\partial u^j}{\partial v^\beta} \frac{\partial u^k}{\partial v^\gamma}. \quad (22)$$

We use Einstein notation with respect to  $\delta$ . Observe the Ricci tensor is a contraction, and so

$$\widetilde{\text{Ric}}(g)_{\alpha\gamma} = \tilde{R}_{\alpha \ \delta\gamma}^{\delta} = \sum_{i,l,j,k} R_{i \ jk}^l \frac{\partial u^i}{\partial v^\alpha} \frac{\partial v^\delta}{\partial u^l} \frac{\partial u^j}{\partial v^\delta} \frac{\partial u^k}{\partial v^\gamma} \quad (23)$$

$$= \sum_{i,l,j,k} R_{i \ jk}^l \frac{\partial u^i}{\partial v^\alpha} \frac{\partial u^j}{\partial v^\delta} \frac{\partial v^\delta}{\partial u^l} \frac{\partial u^k}{\partial v^\gamma} \quad (24)$$

$$= \sum_{i,l,j,k} R_{i \ jk}^l \tilde{\delta}_{jl} \frac{\partial u^i}{\partial v^\alpha} \frac{\partial u^k}{\partial v^\gamma}, \quad (25)$$

where  $\tilde{\delta}_{jl}$  is the Kronecker delta, which follows from the chain rule and induces a contraction over indices  $(j, l)$ . Hence,

$$\widetilde{\text{Ric}}(g)_{\alpha\gamma} = \sum_{i,l,k} R_{i \ lk}^l \frac{\partial u^i}{\partial v^\alpha} \frac{\partial u^k}{\partial v^\gamma} = \sum_{i,k} \frac{\partial u^i}{\partial v^\alpha} \frac{\partial u^k}{\partial v^\gamma} \sum_l R_{i \ lk}^l, \quad (26)$$

giving the result

$$\widetilde{\text{Ric}}(g)_{\alpha\gamma} = \sum_{i,k} \text{Ric}(g)_{ik} \frac{\partial u^i}{\partial v^\alpha} \frac{\partial u^k}{\partial v^\gamma}. \quad (27)$$

The step using  $\tilde{\delta}_{jl}$  to form a contraction via the chain rule is noted in [hft, 2023], which applies to the Ricci tensor under a coordinate transformation that we see here. Using the above, we can formulate Ricci flow in our objective function in terms of a transformed coordinate system using a Cartesian baseline.

Ricci flow under a coordinate transformation holds value when considering special cases of metrics under an alternative coordinate design over Cartesian coordinates. One may be interested in a manifold defined over a domain parameterized in Cartesian coordinates, which may offer certain computational advantages, while the metric coefficients or other useful properties of the manifold are governed by an alternative coordinate system.

Closed forms of quantities under coordinate transformations are occasionally well known, but that of the Ricci tensor holds less renown, giving value to what we show here.

## D Special cases

Special cases can be under consideration, which offer various advantages. The primary of which is reduction in computational power necessary to conduct the learning, which in turn permits higher dimensional structures for more expressive representations. Specifications can be made that consolidate the possibilities of the manifold into a single structure, which generally constrain the problem to yield sub-optimality, but also gain computational favor in the learning stage and yield possibly desirable results, especially if the manifold accords well with the PDE data.

Our special cases will be constraining the metric in one that is known, i.e. inherent to an exact and known manifold, using a known solution to Ricci flow via the manifold equation itself given a domain of parameterization, and a restriction to surfaces of revolution. One can extend special cases more generally, such as in using different coordinate systems, in which the result of Appendix C is useful.

### D.1 Setting a known metric

In this setting, we specify a scenario with a known metric such that Ricci flow is satisfied. We will examine the cigar soliton, with initial metric given by

$$g_0 = g(u, 0) = \frac{du^1 \otimes du^1 + du^2 \otimes du^2}{1 + (u^1)^2 + (u^2)^2} \quad (28)$$

which can be solved and extended for all times under Ricci flow. The cigar soliton metric for general times can be solved as in [Hénot, 2019], which yields the metric

$$g(u, t) = \frac{du^1 \otimes du^1 + du^2 \otimes du^2}{e^{4t} + (u^1)^2 + (u^2)^2}. \quad (29)$$

This metric replaces the metric neural network  $g_{\theta_g}$  implementation within the loss function, as well as the use of Ricci flow upon  $g_{\theta_g}$  in the physics-informed setting. Now, we match the inner product of the tangent vectors upon  $\mathcal{E}_{\theta_\varepsilon}$  with this fixed metric directly.

Our optimization problem becomes the loss minimization framework

$$\min_{\theta \in \Theta} \mathbb{E}_t \mathbb{E}_\Phi \left[ \frac{1}{N} \sum_j |\mathcal{D}_{\theta_D, j}(\mathcal{E}_{\theta_\varepsilon}(u, \hat{\tau})) - \phi_j|^2 \right] \quad (30)$$

$$+ \mathbb{E}_t \mathbb{E}_\Phi \left[ \frac{1}{2} \sum_{j=1}^2 |(e^{4\hat{\tau}} + \|u\|_2^2)^{-1} - \|\partial_j \mathcal{E}_{\theta_\varepsilon}(u, \hat{\tau})\|_2^2|^2 \right] \quad (31)$$

$$+ \mathbb{E}_t \mathbb{E}_\Phi [|\langle \partial_1 \mathcal{E}_{\theta_\varepsilon}(u, \hat{\tau}), \partial_2 \mathcal{E}_{\theta_\varepsilon}(u, \hat{\tau}) \rangle|^2]. \quad (32)$$

The first term is that to match the PDE solution, and the second and third are to enforce the cigar soliton manifold constraint. The loss function may be transformed for any fixed metric, generally minimizing the loss between the metric and  $(J\mathcal{E}_{\theta_\varepsilon}(u, \hat{\tau}))^T (J\mathcal{E}_{\theta_\varepsilon}(u, \hat{\tau}))$ , being the matrix of inner products of the tangent vectors, that we saw previously.

Another option is the torus, which has metric [Jain et al., 2022]

$$g(u, t) = (b + a \cos(u^2))^2 du^1 \otimes du^1 + a^2 du^2 \otimes du^2 \quad (33)$$

over domain  $u^1 \times u^2 \in [0, 2\pi] \times [0, 2\pi]$ . We will specify  $b = 2, a = -1$ . As with the cigar soliton, the matrix of the inner product of the tangent vectors can be matched with the fixed metric in training. A loss function similar to 30, 31 can be formulated with this metric; however, we remark this metric is independent of time, and the solution is learned purely by the displacement of the manifold through the embedding rather than through the flow.

One can enforce symmetry constraints upon the torus by the addition of the terms

$$\mathbb{E}_t \mathbb{E}_\Phi [|(J\mathcal{E}_{\theta_\varepsilon}(u^1, u^2, \hat{\tau}))^T (J\mathcal{E}_{\theta_\varepsilon}(u^1, u^2, \hat{\tau}))| \quad (34)$$

$$- (J\mathcal{E}_{\theta_\varepsilon}(u^1 + \delta, u^2, \hat{\tau}))^T (J\mathcal{E}_{\theta_\varepsilon}(u^1 + \delta, u^2, \hat{\tau}))|_F^2] \quad (35)$$

$$+ \mathbb{E}_t \mathbb{E}_\Phi [|(J\mathcal{E}_{\theta_\varepsilon}(u^1, u^2, \hat{\tau}))^T (J\mathcal{E}_{\theta_\varepsilon}(u^1, u^2, \hat{\tau}))| \quad (36)$$

$$- (J\mathcal{E}_{\theta_\varepsilon}(u^1, 2\pi - u^2, \hat{\tau}))^T (J\mathcal{E}_{\theta_\varepsilon}(u^1, 2\pi - u^2, \hat{\tau}))|_F^2] \quad (37)$$

to the loss, using the symmetry conditions for the torus  $g(u^1, u^2, \hat{\tau}) = g(u^1 + \delta, u^2, \hat{\tau})$ ,  $g(u^1, u^2, \hat{\tau}) = g(u^1, 2\pi - u^2, \hat{\tau})$  for  $\delta \in [0, 2\pi]$  [Jain et al., 2022].

We present some computational results on the Burger’s equation experiment in such settings. It is meaningful to compare to observe optimality of geometry, as such acts as a means of displaying how different geometries produce different results.

1-d Burger’s equation learning for fixed metrics					
method	$t = 0$	$t = 0.25$	$t = 0.5$	$t = 0.75$	$t = 1$
Cigar	$1.38 \pm 2.02$	$1.48 \pm 1.38$	$1.62 \pm 1.64$	$1.61 \pm 1.88$	$2.17 \pm 2.40$
Torus	$1.59 \pm 0.969$	$2.49 \pm 1.23$	$2.68 \pm 1.31$	$2.46 \pm 1.20$	$3.69 \pm 2.49$

Table 6: We examine our method on the Burger’s equation experiment using the cigar soliton solution and the torus. All training details and hyperparameters are kept constant as those in the original experiment aside from the manifold learning.

1-d Burger’s equation extrapolation for fixed metrics			
Method # 1	$\mathcal{A}_1^{new}, t = 0.35$	Method # 2	$\mathcal{A}_1^{new}, t = 0.35$
Cigar	$15.5 \pm 11.3$	Torus	$14.1 \pm 5.76$

Table 7: We examine extrapolation results on our fixed metrics on 30 test sets.

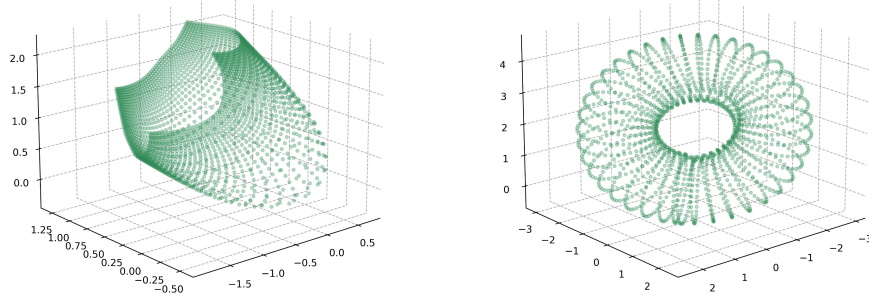


Figure 8: Examples of the cigar soliton and torus learned intrinsically in physics-informed settings. The metrics are fixed and we match the matrices of tangent vector inner products with the known metrics. This figure is purely illustrative, as the parameterization domains  $\mathcal{U}$  are fixed and not learned via a neural network as they would be by learning PDE data. Only the point of the cigar is learned, but the entire torus is learned. In general, for PDE learning, submanifolds are learned.

## D.2 $(d-1)$ -sphere

A manifold evolving according to Ricci flow can be known, in which employing the metric to solve the objective function can be avoided. We will turn our attention to the  $(d-1)$ -dimensional sphere embedded in  $\mathbb{R}^d$ . The  $(d-1)$ -sphere maintains that the fact that it is indeed a sphere subject to Ricci flow, while only the radius changes according to the equation

$$r(t) = \sqrt{R^2 - 2(d-2)t}, \quad (38)$$

for initial radius  $R$  [Sheridan, 2006]. The  $(d-1)$ -sphere manifold parameterization is also known, and given by the parameterized equations [orangesoda, 2013]

$$\mathcal{E}_{\mathbb{S}^{d-1}}^1 = r(t) \cos u^1 \quad (39)$$

$$\mathcal{E}_{\mathbb{S}^{d-1}}^i = r(t) \cos u^i \prod_{j=1}^{i-1} \sin u^j \quad (40)$$

$$\mathcal{E}_{\mathbb{S}^{d-1}}^d = r(t) \prod_{j=1}^{d-1} \sin u^j, \quad (41)$$

where  $i \in \{2, \dots, d-1\}$ , and  $(u^1, \dots, u^{d-1}) = u \in \mathcal{U}$  is still learned via a parameterization neural network  $\mathcal{P}_{\theta_{\mathcal{P}}}$ . A decoder still maps the manifold points to the PDE solution, and so neural networks  $\mathcal{P}_{\theta_{\mathcal{P}}}$  and  $\mathcal{D}_{\theta_{\mathcal{D}}}$  remain while the metric network  $g_{\theta_g}$  is removed, and the encoding network  $\mathcal{E}_{\theta_{\mathcal{E}}}$  replaced.

Our objective function in this setting is greatly simplified, and becomes the risk minimization framework

$$\min_{\theta \in \Theta} \mathbb{E}_t \mathbb{E}_{\Phi} \left[ \frac{1}{N} \sum_j |\mathcal{D}_{\theta_{\mathcal{D}},j}(\mathcal{E}(u, \hat{\tau})) - \phi_j|^2 \right]. \quad (42)$$

The inner product term is removed, as well as the Ricci flow term, which is automatically incorporated into the evaluation involving  $\mathcal{E}$ . This objective function reduces the PDE-solving problem to parameterizing the initial PDE data into the optimal point along the manifold, which evolves and is sequentially decoded.

Formulating the sphere with this method removes the fact that the evolution is governed by an intrinsic flow. In this special case, the sphere is centered at the origin, and so the embedding is fixed. The flow can be made to behave intrinsically in one of two ways.

The first way is to allow the sphere to shift the center away from the origin. This allows the evolution to behave similarly to how it would during an intrinsic flow. This can be done by constructing a new neural network  $\mathcal{S}_{\theta_S} : [0, \tau] \times \Theta_S \rightarrow \mathbb{R}^d$ , which displaces the sphere in the embedding based on time. This displacement is taken for all points along the sphere such that the center of the sphere is moved. This can be done using

$$\tilde{\mathcal{E}}_{\mathbb{S}^{d-1}}^i = \mathcal{E}_{\mathbb{S}^{d-1}}^i + \mathcal{S}_{\theta_S}^i, \quad (43)$$

where  $\tilde{\mathcal{E}}$  is the new sphere after the change of centers. Observe  $\mathcal{E}_{\mathbb{S}^{d-1}}$  is the fixed sphere at the center and  $\mathcal{S}_{\theta_S}$  is learned in training. We denote  $i$  as the  $i$ -th coordinate in  $\mathbb{R}^d$ .

The second way is to utilize the known metric of the  $(d-1)$ -sphere, and solve for the manifold with an encoding neural network as we did in D.1 via the inner product and metric relation. The metric of the  $(d-1)$ -sphere is given as [orangesoda, 2013]

$$g = r(t)^2 du^1 \otimes du^1 + r(t)^2 \sum_{i=2}^{d-1} \left( \prod_{j=1}^{i-1} \sin^2 u^j \right) du^i \otimes du^i. \quad (44)$$

### D.3 Surfaces of revolution

Surfaces of revolution tend to pair well with periodic data, such as instances of periodicity corresponding to circular and torus-like topologies [Lopez and Atzberger, 2022]. Furthermore by adding such a restriction and designing the neural networks in such a fashion to be suitable for a surface of revolution, computational gains are to be made, like with other special cases. While Ricci flow is an intrinsic flow, a manifold being a surface of revolution indeed is an extrinsic quality, in which our intrinsic methodology becomes one that is extrinsic in this special case.

A surface of revolution that is time-dependent is a manifold that takes the form

$$\hat{\mathcal{E}}(u^1, u^2, \hat{\tau}) = (r(u^1, \hat{\tau}) \cos(u^2), r(u^1, \hat{\tau}) \sin(u^2), z(u^1, \hat{\tau})). \quad (45)$$

In this framework, we bypass the need to parameterize an encoder and a metric, and instead we parameterize two neural networks

$$r_{\theta_r} = r : \mathcal{U}^1 \times [0, \tau] \times \Theta_r \rightarrow \mathbb{R}^+, \quad (46)$$

$$z_{\theta_z} = z : \mathcal{U}^1 \times [0, \tau] \times \Theta_z \rightarrow \mathbb{R}, \quad (47)$$

where  $\mathcal{U}^1 \times \mathcal{U}^2 = \mathcal{U} \subseteq \mathbb{R}^2$  is the parameterization domain, and  $\Theta_r, \Theta_z$  are finite-dimensional parameter spaces.

A result proves that Ricci flow preserves symmetries found in the original metric  $g_0$  and manifold  $\mathcal{M}_0$  [Calegari, 2023], meaning that a surface of revolution subject to Ricci flow maintains the fact that it indeed remains a surface of revolution throughout its evolution, i.e. symmetry is preserved. Such results in the fact that the form of equation 45 holds over its evolution. Furthermore, a surface of revolution has a fixed metric that is consequently known over this period, which is given by [Millman and Parker, 1977]

$$g = [(\partial_{u^1} r_{\theta_r}(u^1, \hat{\tau}))^2 + (\partial_{u^1} z_{\theta_z}(u^1, \hat{\tau}))^2] du^1 \otimes du^1 + r_{\theta_r}(u^1, \hat{\tau})^2 du^2 \otimes du^2, \quad (48)$$

using the neural networks in the metric. To solve Ricci flow, one need evaluate the Ricci tensor, which can be formulated from the Christoffel symbols which have a closed form under such a metric [Arapura]:

$$\Gamma_{11}^1 = \frac{(\partial_{u^1} r_{\theta_r})(\partial_{u^1}^2 r_{\theta_r}) + (\partial_{u^1} z_{\theta_z})(\partial_{u^1}^2 z_{\theta_z})}{(\partial_{u^1} r)^2 + (\partial_{u^1} z)^2}, \quad (49)$$

$$\Gamma_{22}^1 = -\frac{r_{\theta_r} \partial_{u^1} r_{\theta_r}}{(\partial_{u^1} r)^2 + (\partial_{u^1} z)^2} \quad (50)$$

$$\Gamma_{12}^1 = \Gamma_{21}^2 = \frac{\partial_{u^1} r_{\theta_r}}{r_{\theta_r}}, \quad \Gamma_{11}^2 = \Gamma_{12}^1 = \Gamma_{21}^1 = \Gamma_{22}^2 = 0. \quad (51)$$

Our training objective function is transformed into

$$\min_{\theta \in \Theta} \mathbb{E}_t \mathbb{E}_\Phi [|\partial_t(\partial_{u^1} r_{\theta_r}(u^1, \hat{\tau}))^2 + \partial_t(\partial_{u^1} z_{\theta_z}(u^1, \hat{\tau}))^2 + 2(\text{Ric}(g))_{11}|^2] \quad (52)$$

$$+ \mathbb{E}_t \mathbb{E}_\Phi [|\partial_t r_{\theta_r}(u^1, \hat{\tau})^2 + 2(\text{Ric}(g))_{22}|^2] \quad (53)$$

$$+ \mathbb{E}_t \mathbb{E}_\Phi [2(\text{Ric}(g))_{12}|^2 + |2(\text{Ric}(g))_{21}|^2] \quad (54)$$

$$+ \mathbb{E}_t \mathbb{E}_\Phi \left[ \frac{1}{N} \sum_j |\mathcal{D}_{\theta_{\mathcal{D}},j}(r_{\theta_r}(u^1, \hat{\tau}) \cos(u^2), r_{\theta_r}(u^1, \hat{\tau}) \sin(u^2), z_{\theta_z}(u^1, \hat{\tau})) - \phi_j|^2 \right]. \quad (55)$$

To formulate the Ricci tensor, one can avoid analytic derivatives of the Christoffel symbols via automatic differentiation.

## E Comparable methodology

The Riemannian tensor can additionally be computed using the coefficients of the second fundamental form [Millman and Parker, 1977], bypassing the need of Christoffel symbols. The coefficients of the second fundamental form are a collection  $\{L_{ij}\}_{i,j=1}^{\dim(\mathcal{U})}$  defined as

$$L_{ij}(t) = \langle \partial_{ij}^2 \mathcal{E}(u, t), n(t) \rangle \quad (56)$$

where  $\mathcal{E}$  is the manifold function taken with neural network  $\mathcal{E} = \mathcal{E}_{\theta_\mathcal{E}}$ ,  $u \in \mathcal{U}$  belongs to a parameterization domain, and  $\partial_\ell$  denotes the partial derivative with respect to  $u^\ell$ .  $n$  is the vector normal to the surface, i.e.

$$n(t) = \frac{\partial_1 \mathcal{E}(u, t) \times \partial_2 \mathcal{E}(u, t)}{\|\partial_1 \mathcal{E}(u, t) \times \partial_2 \mathcal{E}(u, t)\|_2} \quad (57)$$

when  $\mathcal{U} \subseteq \mathbb{R}^2$ . The Riemannian tensor can be formulated as

$$R_{i \ jk}^l = L_{ik} L_j^l - L_{ij} L_k^l. \quad (58)$$

where we use

$$L_k^l = \sum_i L_{ik} g^{il}, \quad (59)$$

where the metric coefficients  $g_{ij}$  can be computed directly from the manifold  $\mathcal{E}$  as in equation 4. Hence, we can circumvent the use of a physics-informed neural network for the metric  $g_{\theta_g}$ , and substitute the Riemannian tensor directly into the Ricci flow equation [Li and Lu, 2017] for a residual. Ricci flow with the above formulation becomes

$$\partial_t \langle \partial_i \mathcal{E}, \partial_j \mathcal{E} \rangle = -2 \sum_l (L_{ij} L_l^l - L_{il} L_j^l). \quad (60)$$

where the indices  $(i, j)$  correspond to that that would be of the metric. The residual to minimize in the objective function to ensure the satisfaction of Ricci flow becomes

$$\mathcal{L}_{Ric}(\theta) = \mathbb{E}_t \mathbb{E}_\Phi \left[ \sum_i \sum_j |\partial_t \langle \partial_i \mathcal{E}(u, \hat{\tau}), \partial_j \mathcal{E}(u, \hat{\tau}) \rangle + 2 \sum_l (L_{ij} L_l^l - L_{il} L_j^l)|^2 \right], \quad (61)$$

where the summation over  $(i, j)$  runs over the indices corresponding to the metric, and the summation over  $l$  runs over the contraction of the Ricci tensor with respect to the Riemannian tensor. The term  $\mathcal{L}_{met}(\theta)$  is omitted in the loss minimization framework in this strategy.

This alternative methodology is comparable to that in which we previously established. It is approximately equally computationally expensive, distinguished by the amount of terms to be differentiated, and it additionally requires a parameterization domain  $\mathcal{U}$ , typically low-dimensional to formulate the normal vector as a cross product; however, we remark it is worthy to realize what we formerly proposed can be reformulated in such a way, perhaps to be extended in future work.

## F Augmented architecture

In this section, we describe the modified multilayer perceptron architecture as in [Wang et al., 2021] for our diffusion-reaction experiment. Denote  $\sigma(\cdot)$  a twice continuously differentiable activation function, and denote  $\zeta$  neural network input. We first pass input  $\zeta$  into two layers  $\hat{\zeta} = \sigma(\tilde{W}\zeta + \tilde{b})$ ,  $\tilde{\zeta} = \sigma(\tilde{W}\zeta + \tilde{b})$ . The architecture proceeds iteratively as

$$\zeta^{i+1} = (1 - \sigma(W^i \zeta^i + b^i)) \odot \hat{\zeta} + \sigma(W^i \zeta^i + b^i) \odot \tilde{\zeta}, \quad (62)$$

where the first iterate is given by  $\zeta^1 = \sigma(W^0 \zeta + b^0)$ , and  $\odot$  denotes element-wise multiplication. Quantities  $W^i, b^i$  denote neural network weights and biases.

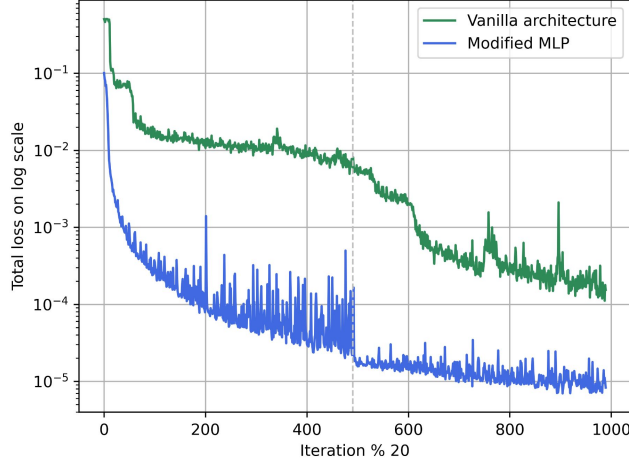


Figure 9: We compare training loss with the modified MLP architecture versus a vanilla architecture used in the diffusion-reaction experiment. The learning rate was adjusted after 10,000 iterations (dashed gray line). The first handful of iterations are omitted to better demonstrate the overall training.

## G Additional experimental details

We assess our experiments using relative  $L^1$  error upon predicted solutions and base data, using the metric

$$\mathbb{E}_{\Phi} \left[ \frac{\|\mathcal{D}_{\theta_{\mathcal{D}}}(\mathcal{E}_{\theta_{\mathcal{E}}}(u, \hat{\tau})) - \phi_{\hat{t}}\|_{L^1(\mathcal{X})}}{\|\phi_{\hat{t}}\|_{L^1(\mathcal{X})}} \right], \quad (63)$$

at time  $\hat{t}$  corresponding to Ricci flow time  $\hat{\tau}$ , where an empirical average is taken to approximate the expected value. This metric behaves as a percentage error.

The primary means of facilitating the training process focuses on differentiation of the Christoffel symbols, i.e.  $\partial_j \Gamma_{ik}^l$ , which is nontrivial via automatic differentiation in a recurring training procedure, and adds significant time to the training process. This can mostly be resolved by differentiating each term involved in the Christoffel symbol calculation individually, and then forming the derivatives  $\partial_j \Gamma_{ik}^l$  afterwards. This resulted in speeding up training by approximately  $\times 3$ . When constructing our derivatives numerically, we first compute all second-order derivatives of the metric and then construct the Christoffel symbols from the derivatives of these terms via product rule, i.e.

$$\partial_j \Gamma_{ik}^l = \frac{1}{2} \sum_{p=1}^2 (\partial_j g^{pl} (\partial_k g_{ip} - \partial_p g_{ik} + \partial_i g_{pk}) + g^{pl} (\partial_{kj} g_{ip} - \partial_{pj} g_{ik} + \partial_{ij} g_{pk})). \quad (64)$$

## H Additional figures

### H.1 Burger's equation

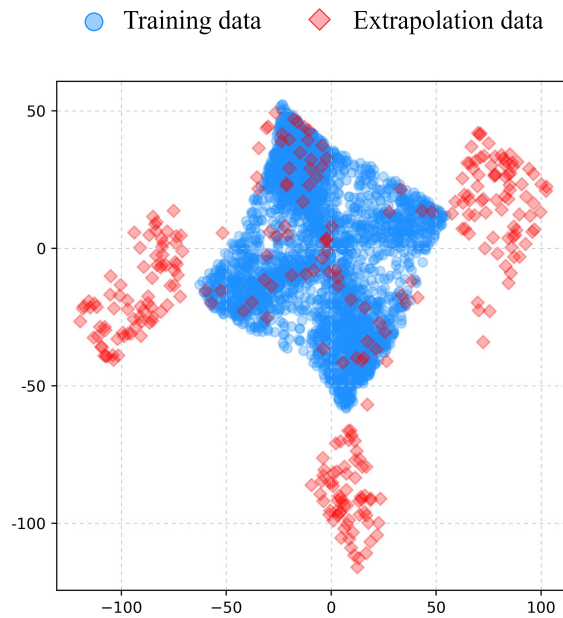


Figure 10: We view training and extrapolation data as points in parameterization domain  $\mathcal{U}$ .

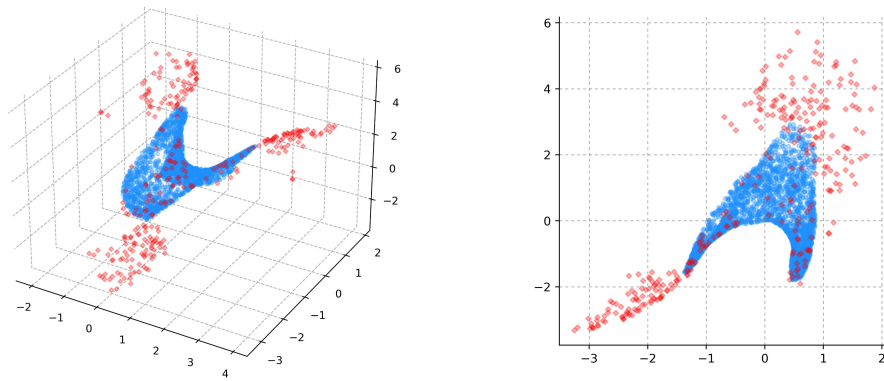


Figure 11: We view training and extrapolation data as points along the manifold at  $t = 0.5$ . The right image is a projection on the  $yz$ -axis.

## H.2 Diffusion-reaction equation

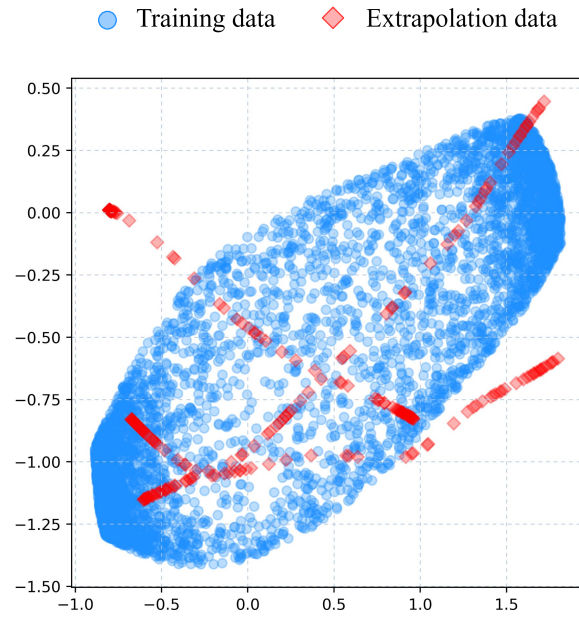


Figure 12: We view training and extrapolation data as points in parameterization domain  $\mathcal{U}$ .

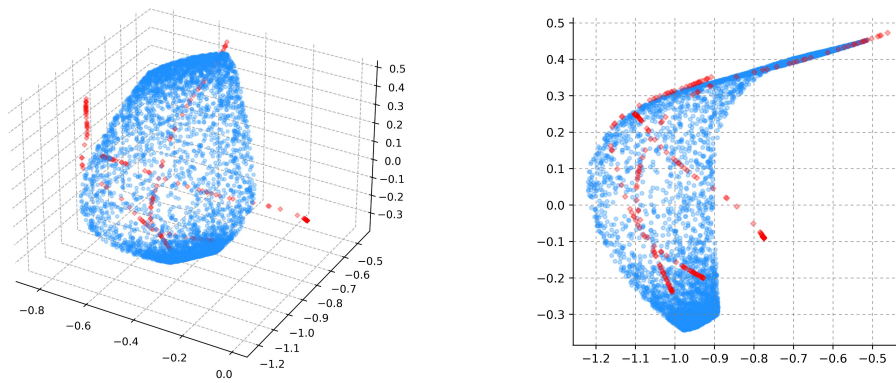


Figure 13: We view training and extrapolation data as points along the manifold at  $t = 0.5$ . The right image is a projection on the  $yz$ -axis.